Revisiting theoretical analysis of the electric dipole moment of ^{129}Xe

B. K. Sahoo [1,*] Nodoka Yamanaka [2,3] and Kota Yanase [3]

[1]*Atomic, Molecular and Optical Physics Division, Physical Research Laboratory, Navrangpura, Ahmedabad 380009, India*
[2]*Kobayashi-Maskawa Institute for the Origin of Particles and the Universe, Nagoya University, Nagoya 464-8602, Japan*
[3]*Nishina Center for Accelerator-Based Science, RIKEN, Wako 351-0198, Japan*

The linear response approach to the relativistic coupled-cluster (RCC) theory has been extended to estimate contributions from the parity and time-reversal violating pseudoscalar-scalar (Ps-S) and scalar-pseudoscalar (S-Ps) electron-nucleus interactions along with electric dipole moments (EDMs) of electrons (d_e) interacting with internal electric and magnetic fields. The random phase approximation (RPA) is also employed to produce results to compare with the earlier reported values and demonstrate the importance of the non-RPA contributions arising through the RCC method. It shows that contributions from the S-Ps interactions and d_e arising through the hyperfine-induced effects are very sensitive to the contributions from the high-lying virtual orbitals. Combining atomic results with the nuclear shell-model calculations, we impose constraints on the pion-nucleon coupling coefficients, and the EDMs of a proton and a neutron. These results are further used to constrain EDMs and chromo-EDMs of the up- and down-quarks by analyzing particle physics models.

I. INTRODUCTION

The search for permanent electric dipole moments (EDMs) due to parity and time-reversal symmetry violating (P,T-odd) interactions is one of the most interesting phenomena today, yet very challenging to observe in either elementary particles or composite systems [1,2]. One of the biggest cosmological mysteries in our universe is the riddle of matter-antimatter asymmetry [3–5]. This can be explained through enough charge conjugation and parity (CP) symmetry violating sources in nature that arise especially from the leptonic and semileptonic sources. Observations of EDMs would lead to CP violation for a wide range of sources [6]. The Standard Model (SM) of particle physics describes CP violation via a complex phase in the Cabibbo-Kobayashi-Maskawa matrix [7], but it cannot explain the large matter-antimatter asymmetry observed in the Universe. Direct probes of EDMs on elementary particles will remain almost impossible in the next few decades as they demand energies that are beyond the reach of very large energy facilities, such as the Large Hadron Collider (LHC) at CERN, owing to Heisenberg's uncertainty principle. Since EDMs of composite objects are enhanced due to electron correlation effects, atoms and molecules are used as proxies over elementary particles to fathom CP-violating phenomena associated at the fundamental level. Although the SM predicts very small values for atomic EDMs [8–11], the actual sizes could be much larger as predicted by many models beyond the SM (BSM). One would expect different types of sources of P,T-odd interactions apart from the hadronic interactions predicted by the SM within the atomic and molecular systems [12–16]. They can arise through the interactions among the quarks, electrons, and electrons and quarks.

Depending on the nature of the interactions, their roles become significant in a particular atomic system. Atomic EDM due to the electron EDMs or the P,T-odd scalar-pseudoscalar (S-Ps) electron-nucleon (e-N) interactions in diamagnetic atoms are quite small and usually neglected in the analysis. However, they can give dominant contributions to the EDM of a paramagnetic system. Similarly, nuclear Schiff moment (NSM) and tensor-pseudotensor (T-Pt) e-N interactions can give significant contributions to the EDM of a diamagnetic system. The former arises due to CP-violating quark-gluon level interactions, such as the EDMs and chromo-EDMs of quarks. The latter is due to the T-Pt electron-quark (e-q) interaction originating from the T-Pt electron-quark interaction, which has been predicted by the leptoquark models [17–22].

The analysis of contributions from all possible sources of P,T-odd interactions to a particular atomic system can be quite useful. Since these interactions contribute with different proportion to the EDMs of various atomic systems, it would be possible to distinguish the source of each type of P,T-odd interaction unambiguously by combining the calculations and measurements of the EDMs of a number of atomic systems. We intend to rigorously estimate the contributions from the many plausible sources of P,T-odd interactions to the EDM of the ^{129}Xe atom. As mentioned above, the EDMs and chromo-EDMs of quarks as well as T-Pt e-q coefficients can be deduced from the EDM study of the ^{129}Xe atom. Compared to other diamagnetic systems, the nuclear structure of ^{129}Xe can be easily analysed theoretically. Moreover, there are three experiments underway on the measurement of the EDM of ^{129}Xe [23–25]. Apart from the T-Pt e-N interactions and the NSM, the other possible sources of P,T-odd interactions that can contribute to the EDM of a diamagnetic system including ^{129}Xe atom at the leading order are the pseudoscalar-scalar (Ps-S) e-N interactions, the S-Ps e-N interactions, and the electron EDM (d_e) interacting with internal electric and magnetic fields

*bijaya@prl.res.in

[26,27]. Contributions from the Ps-S e-N interactions and d_e interacting with the internal magnetic field can be realized at the same level of perturbation as the T-Pt e-N interactions and the NSM to the EDM of the diamagnetic atoms, but their magnitudes are quite small compared to the latter two interactions owing to the fact they are inversely proportional to the mass of a proton. On the other hand, the S-Ps e-N interactions and d_e interacting with the internal electric field will not contribute to the EDM of a diamagnetic system at the second order of perturbation because their corresponding interaction Hamiltonians are in the scalar form and the ground state of diamagnetic atoms has null angular momentum. Thus, the leading-order contributions from these interactions can arise through the interactions with the magnetic dipole hyperfine ($M1_{\rm hf}$) structure interactions. As a consequence, contributions from these interactions are also small to the EDMs of the diamagnetic atoms.

Earlier, contributions from the T-Pt e-N interactions and NSM to ^{129}Xe were rigorously estimated by employing the relativistic coupled-cluster (RCC) theory in both the linear response [28] and biorthogonal [29] approaches, which showed that the results from both of the approaches almost agree with each other. In this work, we again estimate contributions from the T-Pt e-N interactions and the NSM, along with contributions from the Ps-S e-N interactions and d_e interacting with nuclear magnetic field. We have employed the random phase approximation (RPA) and linear response RCC theory to demonstrate the convergence of their values with the basis size and by comparing results with the previous calculations. Then, we extend these approaches considering $M1_{\rm hf}$ as an additional perturbation to account for the contributions from the S-Ps e-N interactions and d_e interacting with the internal electric field. We find that the convergence of the results with respect to basis functions without and with the presence of $M1_{\rm hf}$ are very different. As a result, our estimated contributions from the hyperfine-induced effects differ substantially from the earlier estimations.

II. PARTICLE PHYSICS

We can write the effective P,T-odd Lagrangian at the e-N interaction level as [13]

$$\mathcal{L}_{\rm eff}^{\rm PT} = \mathcal{L}_e + \mathcal{L}_p + \mathcal{L}_n + \mathcal{L}_{\pi NN} + \mathcal{L}_{eN}, \tag{1}$$

where $\mathcal{L}_e$ denotes contributions from electron EDMs, $\mathcal{L}_p$ denotes contributions from proton EDMs, $\mathcal{L}_n$ denotes contributions from neutron EDMs, $\mathcal{L}_{\pi NN}$ represents contributions from the pion-nucleon-nucleon (π-N-N) interactions, and $\mathcal{L}_{eN}$ gives contributions from the e-N interactions. Here we do not consider the short-range CP-odd nucleon-nucleon interaction which *a priori* gives the leading contribution for the chiral symmetry nonviolating CP-odd quark-gluon level interaction [30,31]. It is actually known from several nuclear level *ab initio* calculations that the short-range CP-odd force yields much smaller effects than the pion-exchange ones induced by $\mathcal{L}_{\pi NN}$ [32–35]. This is qualitatively explained by the spin dependence of the CP-odd nuclear force. Since the ground states of ordinary odd nuclei have only one unpaired nucleon, the short-range CP-odd nuclear force only acts in the vicinity of this single nucleon, whereas the pion-exchange interaction

can interact with more nucleons thanks to its long-range nature.

The relativistic expression for the EDM interaction of a spin-1/2 fermion f ($= e, p, n$) is given by

$$\mathcal{L}_f = -\frac{i}{2} d_f \bar{\psi}_f F_{\mu\nu} \sigma^{\mu\nu} \gamma_5 \psi_f, \tag{2}$$

where $F_{\mu\nu}$ is the field strength of the applied electromagnetic field, $\sigma_{\mu\nu} = \frac{i}{2}[\gamma_\mu, \gamma_\nu]$ with γ's as the Dirac matrices, and ψ_f denotes the Dirac wave function of f. The EDM of quarks mainly generates the nucleon EDM. Recent lattice quantum chromodynamics (QCD) calculations yield [36–41]

$$d_p \approx 0.63 \, d_u|_{\mu=1\,{\rm TeV}} - 0.16 \, d_d|_{\mu=1\,{\rm TeV}}$$

and

$$d_n \approx 0.63 \, d_d|_{\mu=1\,{\rm TeV}} - 0.16 \, d_u|_{\mu=1\,{\rm TeV}}, \tag{3}$$

where d_u and d_d are the up- and down-quark EDMs renormalized at $\mu = 1$ TeV [15,42]. The extraction from the experimental data is also consistent with this value [43], so we assign an uncertainty of 10%. The nucleon EDM receives a contribution from other interactions, but we neglect them since these mainly contribute to the atomic EDM via the P,T-odd π-N-N interactions.

The expression for $\mathcal{L}_e$ is given by

$$\mathcal{L}_e = -\frac{i}{2} d_e \bar{\psi}_e F_{\mu\nu} \sigma^{\mu\nu} \gamma_5 \psi_e. \tag{4}$$

The Lagrangian for the P,T-odd π-N-N interactions that significantly contribute to the EDMs of the diamagnetic atoms is given by [13,44–46]

$$\mathcal{L}_{\pi NN} = \bar{g}_{\pi NN}^{(0)} \bar{\psi}_N \tau^i \psi_N \pi^i + \bar{g}_{\pi NN}^{(1)} \bar{\psi}_N \psi_N \pi^0 \\ + \bar{g}_{\pi NN}^{(2)} (\bar{\psi}_N \tau^i \psi_N \pi^i - 3 \bar{\psi}_N \tau^3 \psi_N \pi^0), \tag{5}$$

where the couplings $\bar{g}_{\pi NN}^{(I)}$ ($I = 0, 1, 2$) with the superscript $i = 1, 2, 3$ represent the isospin components. Up to mass dimension-6, $\mathcal{L}_{\pi NN}$ is generated by the quark-gluon level CP-odd Lagrangian

$$\mathcal{L}_{\rm QCDCPV} = \left(\frac{N_q \bar{\theta} \alpha_s}{16\pi} \epsilon_{\mu\nu\rho\sigma} G_a^{\mu\nu} G_a^{\rho\sigma} \right) - \sum_q^{N_q} \frac{i g_s \tilde{d}_q}{2} \bar{\psi}_q \sigma_{\mu\nu} \\ \times G_a^{\mu\nu} t_a \gamma_5 \psi_q + \frac{w}{6} f^{abc} \epsilon^{\alpha\beta\gamma\delta} G_{\mu\alpha}^a G_{\beta\gamma}^b G_\delta^{\ \mu,c}, \tag{6}$$

where the quarks q are summed over the number of active flavors, N_q, and $G_{\mu\nu}^a$ is the field strength of the gluon with the QCD coupling g_s. Here we do not consider the CP-odd four-quark interaction, which is effectively a dimension-8 operator, due to the Higgs field insertion.

The first term of Eq. (6) is the so-called θ term, which we put in parentheses because it is likely to be unphysical, as recently shown [47–50]. Here, we write its contribution to the isoscalar CP-odd pion-nucleon interaction that was derived using the chiral perturbation theory [13,16,51,52],

$$\bar{g}_{\pi NN}^{(0)} \approx (0.015 \, \bar{\theta}). \tag{7}$$

This expression is just to let the readers know that it was believed that there were unnaturally tight constraints on $\bar{\theta}$, known as the strong CP problem, which can be resolved if it

is unphysical. We also do not consider the Weinberg operator w [last term of Eq. (6)] for which the hadron level matrix elements have large uncertainties [35,53,54].

The contribution of the quark chromo-EDM $\tilde{d}_q$ also has a large uncertainty, although much of effort has been expended in lattice QCD [55,56]. The leading process of $\tilde{d}_q$ contributing to the NSM is most probably the so-called vacuum alignment effect [13,57], which consists of creating a neutral pion from the vacuum by CP-odd operators. According to chiral perturbation, this generates an isovector CP-odd π-N-N interaction [54,58–60],

$$\bar{g}_{\pi NN}^{(1)}(\tilde{d}_q) \approx -\left[\frac{\sigma_{\pi N}}{f_\pi^2 m_\pi^2} + \frac{5g_A^2 m_\pi}{64\pi f_\pi^4}\right]\frac{f_\pi m_\pi^2 m_0^2}{2(m_u + m_d)}(\tilde{d}_u - \tilde{d}_d)$$

$$\approx (125 \pm 75)[\tilde{d}_d|_{\mu=1\,\text{TeV}} - \tilde{d}_u|_{\mu=1\,\text{TeV}}]\,\text{fm}^{-1}, \quad (8)$$

where $m_\pi = 138$ MeV, $f_\pi = 93$ MeV, and $g_A = 1.27$. The quark masses are $m_u = 2.9$ MeV and $m_d = 6.0$ MeV at the renormalization point $\mu = 1$ GeV [8]. We also use the mixed condensate $m_0^2 \equiv \langle 0|\bar{\psi}_q g_s \sigma_{\mu\nu} F_a^{\mu\nu} t_a \psi_q|0\rangle/\langle 0|\bar{q}q|0\rangle = (0.8 \pm 0.2)$ GeV^2 determined using the QCD sum rules [61–63]. The chromo-EDM couplings are renormalized at $\mu = 1$ TeV [15,42]. The uncertainty of the pion-nucleon sigma term, $\sigma_{\pi N} = (45 \pm 15)$ MeV, is dominated by the systematics due to the differences between the lattice results [36,41,64,65] and phenomenological extractions [66,67]. The quoted error bar of 60% is a conservative one. We note that the isoscalar CP-odd coupling $g_{\pi NN}^{(0)}$ is not enhanced by $\sigma_{\pi N}$. The isotensor coupling $g_{\pi NN}^{(2)}$ is also suppressed by the light quark mass factor. For these reasons, we only consider the isovector coupling $g_{\pi NN}^{(1)}$ as regards the chromo-EDM.

The leading P,T-odd Lagrangian for e-N interaction is given by [13]

$$\mathcal{L}_{eN} = -\frac{G_F}{\sqrt{2}}\sum_N\Big[C_S^{eN}\bar{\psi}_N\psi_N\,\bar{\psi}_e i\gamma^5\psi_e$$
$$+ C_P^{eN}\bar{\psi}_N i\gamma^5\psi_N\,\bar{\psi}_e\psi_e$$
$$- \frac{1}{2}C_T^{eN}\varepsilon^{\mu\nu\rho\sigma}\bar{\psi}_N\sigma_{\mu\nu}\psi_N\,\bar{\psi}_e\sigma_{\rho\sigma}\psi_e\Big], \quad (9)$$

where G_F is the Fermi constant, $\varepsilon_{\mu\nu\alpha\beta}$ is the Levi-Civita symbol, and $\psi_{N(e)}$ denote the Dirac wave function of the nucleon (electron). Here, C_S^{eN}, C_P^{eN}, and C_T^{eN} denote the S-Ps, Ps-S, and T-Pt e-N interaction coupling constants, respectively. The above $\mathcal{L}_{eN}$ is generated by the CP-odd e-q interaction,

$$\mathcal{L}_{eq} = -\frac{G_F}{\sqrt{2}}\sum_q\Big[C_S^{eq}\bar{\psi}_q\psi_q\,\bar{\psi}_e i\gamma_5\psi_e + C_P^{eq}\bar{\psi}_q i\gamma_5\psi_q\,\bar{\psi}_e\psi_e$$
$$- \frac{1}{2}C_T^{eq}\varepsilon^{\mu\nu\rho\sigma}\bar{\psi}_q\sigma_{\mu\nu}\psi_q\,\bar{\psi}_e\sigma_{\rho\sigma}\psi_e\Big], \quad (10)$$

at the elementary level. The relations between the CP-odd couplings are given by [68]

$$C_S^{ep} \approx 11\,C_S^{eu} + 10\,C_S^{ed},$$
$$C_S^{en} \approx 10\,C_S^{eu} + 11\,C_S^{ed},$$
$$C_P^{ep} \approx 320\,C_P^{eu} - 300\,C_P^{ed},$$
$$C_P^{en} \approx -300\,C_P^{eu} + 320\,C_P^{ed},$$
$$C_T^{ep} \approx 0.63\,C_T^{eu} - 0.16\,C_T^{ed},$$

and

$$C_T^{en} \approx -0.16\,C_T^{eu} + 0.63\,C_T^{ed}, \quad (11)$$

with all e-q couplings renormalized at $\mu = 1$ TeV. The coefficients of C_P^{eq} and C_T^{eq} have 20% of uncertainty, while those of C_S^{eq} have 40%, due to the systematics of the σ term seen above. We do not give the contributions from the strange and heavier quarks, which are affected by large errors.

III. NUCLEAR PHYSICS

The NSM S is related to the P,T-odd π-N-N couplings and the nucleon EDMs as [69,72]

$$S = g\big(a_0\bar{g}_{\pi NN}^{(0)} + a_1\bar{g}_{\pi NN}^{(1)} + a_2\bar{g}_{\pi NN}^{(2)}\big) + b_1 d_p + b_2 d_n, \quad (12)$$

where $g \simeq 13.5$ is known as the strong π-N-N coupling coefficient, and the a's and b's are the nuclear structure-dependent coefficients.

To obtain the constraints on the hadronic P,T-odd couplings, we use the results of nuclear large-scale shell-model (LSSM) calculations. In this model, the nuclear effective Hamiltonian is diagonalized in an appropriate model space. For ^{129}Xe consisting of 54 protons and 75 neutrons, we consider one major shell between the magic numbers 50 and 82, both for the proton and neutron, as the model space. This choice is reasonable to describe the low-energy properties of nuclei. In fact, the LSSM calculations using the effective Hamiltonians SN100PN [70] and SNV [71] successfully reproduce the low-energy spectra and electromagnetic moments in a wide range of nuclei. The NSM coefficients of ^{129}Xe were reported in Refs. [69,73]. In particular, it was found that the NSM coefficient of the neutron EDM, b_2 in Eq. (12), is apparently correlated to the nuclear magnetic moment. This demonstrates the reliability of the LSSM calculations, which reproduce, with reasonable accuracy, the experimental value of the magnetic moment.

The NSM was evaluated as [69,73]

$$S = (0.002d_p + 0.47d_n)\,\text{fm}^2 + \big(-0.038\bar{g}_{\pi NN}^{(0)}$$
$$+ 0.041\bar{g}_{\pi NN}^{(1)} + 0.082\bar{g}_{\pi NN}^{(2)}\big)ge\,\text{fm}^3, \quad (13)$$

where $b_1 = -0.003$ and 0.006 with the effective Hamiltonians SNV and SN100PN, respectively. A simple regression analysis with the magnetic moment yields an uncertainty of 30% for b_2 [69]. We assume the same level of accuracy for the a's in this paper, although the physical origin of their discrepancy between nuclear models is less clear.

For completeness, we compute the nucleon spin matrix element $(\langle\sigma_N\rangle)$ related to the T-Pt interaction in the same framework. We obtain, for the neutron ($N = n$), $\langle\sigma_n\rangle = 0.666$ and 0.658 by using the effective Hamiltonian SN100PN and SNV, respectively. We adopt the mean value $\langle\sigma_n\rangle = 0.66$ in the following discussion. The proton ($N = p$) spin matrix element is computed as $\langle\sigma_p\rangle = 0.002$. Although this value may be model dependent, it is conclusive that the proton matrix element is orders of magnitude smaller than that of the neutron. The KSHELL code has been utilized for the nuclear calculations [74].

IV. ATOMIC PHYSICS

A. Theory

The EDM (d_a) of an atomic system is given as the expectation value of the dipole operator D in its state, i.e., the ground state $|\Psi_0\rangle$ in this case,

$$d_a = \frac{\langle\Psi_0|D|\Psi_0\rangle}{\langle\Psi_0|\Psi_0\rangle}. \quad (14)$$

The single-particle matrix element of D can be found in Eq. (A2). Assuming that a given P,T-odd interaction in an atomic system is sufficiently smaller than the contributions from the electromagnetic interactions, we can consider up to the first order in the P,T-odd interaction with respect to the electromagnetic interactions for the determination of atomic wave functions. This yields

$$|\Psi_0\rangle \simeq |\Psi_0^{(0)}\rangle + \lambda|\Psi_0^{(1)}\rangle, \quad (15)$$

where superscripts 0 and 1 stand for the unperturbed wave function due to the electromagnetic interactions and its first-order correction due to a P,T-odd interaction Hamiltonian (λH_{PT}), respectively. Here, λ represents the perturbative parameter of the corresponding P,T-odd interaction under consideration. In principle, all possible P,T-odd interactions need to be considered simultaneously in the determination of the atomic wave function. However, it will not make any difference in the precision of the results even if we consider one type of P,T-odd interaction at a time and subsequently study their contributions in an atomic system, owing to the fact that the correlations among all these P,T-odd interactions are negligibly small (second-order effects are much smaller than the intended accuracy of the calculations). With the above approximation, we can express

$$d_a \simeq 2\lambda \frac{\langle\Psi_0^{(0)}|D|\Psi_0^{(1)}\rangle}{\langle\Psi_0^{(0)}|\Psi_0^{(0)}\rangle}. \quad (16)$$

Considering all possible Lagrangians described in Sec. II, the net EDM of an atomic system can be estimated as

$$\begin{aligned} d_a &= d_a^e + d_a^p + d_a^n + d_a^{\pi NN} + d_a^{eN} \\ &= d_a^e + d_a^{Sm} + d_a^{eN}, \end{aligned} \quad (17)$$

where superscripts denote contributions to the EDM from the respective source. We have also combined contributions from the proton EDMs, the neutron EDMs, and the π-N-N interactions to the net EDM contribution from the above sources and denote it as d_a^{Sm}, which are encapsulated within the NSM (S).

Considering the nonrelativistic limit, the atomic Hamiltonian accounting contributions from the electron EDM interactions are given by

$$H_{d_e} = 2icd_e \sum_k \beta_k \gamma_k^5 p_k^2 = \sum_k h_k^{d_e}, \quad (18)$$

where c is the speed of light, β and γ^5 are the Dirac matrices, and p is the magnitude of the momentum of the electron. The matrix element of the single-particle operator h^{d_e} of H_{d_e} is given by Eq. (A3), which shows that it is a scalar operator. As a result, Eq. (16) will be zero for the closed-shell system (with total angular momentum $J = 0$) when H_{d_e} is considered as a perturbation. To get a finite value of d_a due to H_{d_e}, it would

be necessary to consider the next leading-order (third-order) interaction that can arise through the $M1_{hf}$ operator, whose matrix element is given by Eq. (A4). In the presence of both P,T-odd and $M1_{hf}$ interactions, we can express an atomic wave function as

$$|\Psi_0\rangle \simeq |\Psi_0^{(0,0)}\rangle + \lambda_1|\Psi_0^{(1,0)}\rangle + \lambda_2|\Psi_0^{(0,1)}\rangle + \lambda_1\lambda_2|\Psi_0^{(1,1)}\rangle, \quad (19)$$

where we use λ_1 and λ_2 as perturbative parameters for the $M1_{hf}$ and H_{PT} operators, respectively. Thus, the unperturbed and perturbed wave functions are denoted with two superscripts—the first superscript counts the order of $M1_{hf}$ and the second superscript counts the order of H_{PT}. In these notations, we can express

$$d_a^e = 2\lambda_1\lambda_2 \frac{\langle\Psi_0^{(0,0)}|D|\Psi_0^{(1,1)}\rangle + \langle\Psi_0^{(1,0)}|D|\Psi_0^{(0,1)}\rangle}{\langle\Psi_0^{(0,0)}|\Psi_0^{(0,0)}\rangle}. \quad (20)$$

Apart from the contribution from d_e interacting with an internal electric field of an atomic system, there will also be another contribution to d_a because of d_e interacting with the magnetic field (B) of the nucleus. Its interacting Hamiltonian is given by

$$H_B = -d_e \sum_k \gamma_k^0 B = \sum_k h_k^B(r). \quad (21)$$

The single-particle matrix element of this Hamiltonian is given by Eq. (A5). It can contribute at the second-order perturbation to EDM as

$$d_a^B \simeq 2\lambda_2 \frac{\langle\Psi_0^{(0,0)}|D|\Psi_0^{(0,1)}\rangle}{\langle\Psi_0^{(0,0)}|\Psi_0^{(0,0)}\rangle}. \quad (22)$$

Thus, contributions to d_a from the e-N interactions can be expressed as

$$d_a^{eN} = d_a^P + d_a^{Sc} + d_a^T, \quad (23)$$

where d_a^P, d_a^{Sc}, and d_a^T stand for the contributions to EDM from the Ps-S, S-Ps, and T-Pt interactions, respectively.

The interaction Hamiltonian, together with $\mathcal{L}_{\pi NN}$, $\mathcal{L}_p$, and $\mathcal{L}_n$ for the atom with nuclear spin $I = 1/2$ such as ^{129}Xe, can be approximately given by [75]

$$\begin{aligned} H_{int}^{NSM} &= \sum_k \frac{3(\mathbf{S}\cdot\mathbf{r})_k}{B}\rho_{nuc}(r) \\ &= \sum_k h_k^{NSM}(r), \end{aligned} \quad (24)$$

where $\rho_{nuc}(r)$ is the nuclear charge density distribution function, $\mathbf{S} = S\frac{\mathbf{I}}{I}$ is the NSM, and $B = \int_0^\infty dr\, r^4 \rho_{nuc}(r)$. The matrix element of $h_k^{NSM}(r)$ is given by Eq. (A6). H_{int}^{NSM} can contribute at the second-order perturbation to EDM as

$$d_a^{Sm} \simeq 2\lambda_2 \frac{\langle\Psi_0^{(0,0)}|D|\Psi_0^{(0,1)}\rangle}{\langle\Psi_0^{(0,0)}|\Psi_0^{(0,0)}\rangle}. \quad (25)$$

The S-Ps interaction Hamiltonian is given by

$$H_{SPs} = \frac{iG_F C_S}{\sqrt{2}} A \sum_k \beta_k \gamma_k^5 \rho_{nuc}(r) = \sum_k h_k^{SPs}, \quad (26)$$

where A is the atomic mass number of the considered atom. The matrix elements of its single-particle operator h^{SPs} are given by Eq. (A7). Here, we defined $C_S \equiv [ZC_S^{ep} + (A - Z)C_S^{en}]/A$. Since the above interaction Hamiltonian is scalar in nature, it will contribute to the EDM of a closed-shell atom through the hyperfine-induced interaction. Thus, it can be evaluated using the expression

$$d_a^{Sc} = 2\lambda_1\lambda_2 \frac{\langle\Psi_0^{(0,0)}|D|\Psi_0^{(1,1)}\rangle + \langle\Psi_0^{(1,0)}|D|\Psi_0^{(0,1)}\rangle}{\langle\Psi_0^{(0,0)}|\Psi_0^{(0,0)}\rangle}. \quad (27)$$

The Ps-S interaction Hamiltonian is given by

$$H_{PsS} = -\frac{G_F C_P}{2\sqrt{2}m_p c} \sum_k \gamma_0 \boldsymbol{\sigma}_{\mathrm{nuc}} \boldsymbol{\nabla}_k \rho_{\mathrm{nuc}}(r)$$
$$= \sum_k h_k^{PsS}(r), \quad (28)$$

where m_p is the mass of a proton and $\boldsymbol{\sigma}_{\mathrm{nuc}} = \sum_n \langle\sigma_n\rangle + \sum_p \langle\sigma_p\rangle$ is the Pauli spin operator for the nucleus. The Ps-S coupling is approximated as $C_P \approx C_P^n$ since the proton matrix element $\langle\sigma_p\rangle$ is small. The matrix element for its single-particle operator h^{PsS} is given by Eq. (A8). The contribution to d_a from the above Hamiltonian is evaluated by

$$d_a^{Ps} \simeq 2\lambda_2 \frac{\langle\Psi_0^{(0,0)}|D|\Psi_0^{(0,1)}\rangle}{\langle\Psi_0^{(0,0)}|\Psi_0^{(0,0)}\rangle}. \quad (29)$$

The T-Pt e-N interaction Hamiltonian for an atomic system is given by [75–77]

$$H_{\mathrm{int}}^{TPt} = i\sqrt{2}G_F C_T \sum_k \left(\boldsymbol{\sigma}_{\mathrm{nuc}} \cdot \gamma_k^0\right)\rho_{\mathrm{nuc}}(r)$$
$$= \sum_k h_k^{TPt}(r), \quad (30)$$

and the matrix element of its single-particle operator is given by Eq. (A9). We can use the approximation $C_T \approx C_T^n$ again thanks to the small proton matrix element. The contribution to d_a from the above Hamiltonian is evaluated by

$$d_a^T \simeq 2\lambda_2 \frac{\langle\Psi_0^{(0,0)}|D|\Psi_0^{(0,1)}\rangle}{\langle\Psi_0^{(0)}|\Psi_0^{(0)}\rangle}. \quad (31)$$

We would like to mention here that the C_P coefficient can be approximately deduced from C_T, and vice versa, using the relation [78]

$$C_P \approx 3.8 \times 10^3 \times \frac{A^{1/3}}{Z}C_T, \quad (32)$$

where Z is the atomic number of the atom. However, the reliability of this relation has not yet been verified. Thus, it would be necessary to infer both of the coefficients separately to test the above relation.

B. Methodology

The RCC method is a nonperturbative theory to a many-body problem. Its notable characteristics are many folds compared to other contemporary many-body methods that are generally employed to carry out calculations of spectroscopic properties. Among them, the main advantages of a RCC method are its formulation that satisfies size-consistent and size-extensivity properties, its ability to account for different types of correlation effects on equal footing (also cross correlations among them), and it captures more physical effects at the given level of approximation compared to other popular many-body methods [79–81]. We employ this theory to estimate the enhancement coefficients due to each of the P,T-odd interactions. The calculation of wave functions of an atomic system necessitates to first obtain a suitable mean-field wave function (reference state), including part of the electron correlation effects, and treat the residual correlation effects as an external perturbation. Thus, evaluating the second- and third-order EDM properties of an atomic system, as discussed in the previous section, means dealing with another source of perturbation along with the residual correlation effects. This makes it challenging to determine the intended properties using the RCC method.

We consider the Dirac-Coulomb (DC) Hamiltonian to determine the unperturbed wave function $|\Psi_0^{(0,0)}\rangle$ due to the dominant electromagnetic interactions, given by

$$H_0 = \sum_i^{N_e} [c\boldsymbol{\alpha} \cdot \boldsymbol{p}_i + c^2\boldsymbol{\beta} + V_{\mathrm{nucl}}(r_i)] + \frac{1}{2}\sum_{i,j}\frac{1}{r_{ij}}, \quad (33)$$

where N_e is the number of electrons, $\boldsymbol{\alpha}$ is the Dirac matrix, $V_{\mathrm{nucl}}(r_i)$ is the nuclear potential, and r_{ij} is the distance between the ith and jth electrons. In the above expression, we have used atomic units (a.u.) in which $\hbar = 1$ and mass of electron $m_e = 1$.

In the RCC theory framework, we can express $|\Psi_0^{(0,0)}\rangle$ due to H_0 as

$$\left|\Psi_0^{(0,0)}\right\rangle = e^{T^{(0,0)}}|\Phi_0\rangle, \quad (34)$$

where $|\Phi_0\rangle$ is the mean-field wave function obtained using the Dirac-Hartree-Fock (DHF) method and the cluster operator $T^{(0,0)}$ is defined as

$$T^{(0,0)} = \sum_{I=1}^{N_e} T_I^{(0,0)} = \sum_{I=1}^{N_e} t_I^{(0,0)}C_I^+, \quad (35)$$

where I represents the number of particle-hole pairs, $t_I^{(0,0)}$ is the unperturbed excitation amplitude, and C_I^+ is the I pair of creation and annihilation operators denoting the level of excitations. In our work, we have considered both singles and doubles approximation in the RCC theory (RCCSD method) by restricting I up to one-particle–one-hole and two-particle–two-hole excitations, i.e., $T^{(0,0)} = T_1^{(0,0)} + T_2^{(0,0)}$. The general $T^{(0)}$ amplitude solving the equations in the RCC theory is given by

$$\langle\Phi_0|C_I^-\overline{H}_0|\Phi_0\rangle = 0, \quad (36)$$

where C_I^- are the adjoint of C_I^+ (referring to deexcitation) and $\overline{H}_0 = e^{-T^{(0,0)}}H_0 e^{T^{(0,0)}} = (H_0 e^{T^{(0,0)}})_l$, with subscript l denoting the linked terms [below, we shall follow the notation $\overline{O} = (Oe^{T^{(0,0)}})_l$ throughout the paper]. Since H_0 has only one-body and two-body terms, $\overline{H}_0$ can have a finite number of terms. In the RCCSD method approximation, we can have two set of

equations for $T_1^{(0,0)}$ and $T_2^{(0,0)}$ as

$$\langle\Phi_0|C_1^-\big(H_0 T_1^{(0,0)}\big)_l|\Phi_0\rangle$$
$$= -\langle\Phi_0|C_1^- H_0 + \big(H_0 T_2^{(0,0)}\big)_l|\Phi_0\rangle$$
$$- \langle\Phi_0|C_1^-\left[H_0 \sum_{n,m} \frac{T_1^{(0,0)n} T_2^{(0,0)m}}{n!m!}\right]_l|\Phi_0\rangle \quad (37)$$

and

$$\langle\Phi_0|C_2^-\big(H_0 T_2^{(0,0)}\big)_l|\Phi_0\rangle$$
$$= -\langle\Phi_0|C_2^- H_0 + \big(H_0 T_1^{(0,0)}\big)_l|\Phi_0\rangle$$
$$- \langle\Phi_0|C_2^-\left[H_0 \sum_{n,m} \frac{T_1^{(0,0)n} T_2^{(0,0)m}}{n!m!}\right]_l|\Phi_0\rangle, \quad (38)$$

where $n, m \geqslant 1$ denote all possible nonlinear terms. The above equations are solved using the Jacobi iterative procedure.

Now considering external perturbations due to $M1_{\text{hf}}$ and H_{PT}, we can express the total Hamiltonian as

$$H = H_0 + \lambda_1 M1_{\text{hf}} + \lambda_2 H_{\text{PT}}. \quad (39)$$

In the RCC theory framework, we can express $|\Psi_0\rangle$ of H in the form similar to the unperturbed wave function as

$$|\Psi_0\rangle = e^T|\Phi_0\rangle. \quad (40)$$

In order to obtain the perturbed wave functions from this expression, we can express

$$T \simeq T^{(0,0)} + \lambda_1 T^{(1,0)} + \lambda_2 T^{(0,1)} + \lambda_1\lambda_2 T^{(1,1)}, \quad (41)$$

where superscript notations are as per Eq. (19). This follows

$$\big|\Psi_0^{(1,0)}\big\rangle = e^{T^{(0,0)}} T^{(1,0)}|\Phi_0\rangle,$$
$$\big|\Psi_0^{(0,1)}\big\rangle = e^{T^{(0,0)}} T^{(0,1)}|\Phi_0\rangle,$$

and

$$\big|\Psi_0^{(1,1)}\big\rangle = e^{T^{(0,0)}}\big(T^{(1,1)} + T^{(1,0)} T^{(0,1)}\big)|\Phi_0\rangle. \quad (42)$$

The amplitudes of the perturbed RCC operators can be obtained as

$$\langle\Phi_0|C_I^-[\overline{H}_0 T^{(1,0)} + \overline{M1}_{hf}]|\Phi_0\rangle = 0,$$
$$\langle\Phi_0|C_I^-[\overline{H}_0 T^{(0,1)} + \overline{H}_{PT}]|\Phi_0\rangle = 0,$$

and

$$\langle\Phi_0|C_I^-\big[\overline{H}_0 T^{(1,1)} + \overline{H}_0 T^{(1,0)} T^{(0,1)}$$
$$+ \overline{M1}_{hf} T^{(0,1)} + \overline{H}_{PT} T^{(1,0)}\big]|\Phi_0\rangle = 0. \quad (43)$$

It should be noted that the first two equations are independent from each other and are solved separately after obtaining $T^{(0,0)}$ amplitudes. These two equations are of similar form with Eq. (36), so they are also solved using the Jacobi iterative procedure. Once the amplitudes of the $T^{(0,0)}$, $T^{(1,0)}$, and $T^{(0,1)}$ operators are known, the amplitudes of the $T^{(1,1)}$ operator are obtained by solving the last equation in the same Jacobi iterative approach. Since $\overline{O}$ contains many nonlinear terms, among which H_0 also contains two-body terms, we use intermediate computational schemes to solve the amplitude

determining equation for $T^{(1,1)}$. We divide $\overline{H}_0$ into effective one-body and two-body terms like the bare Hamiltonian H_0, and store them to further use to solve all three equations. This reduces much computational time to obtain the perturbed RCC operator amplitudes. Due to the limitation in memory of the available computational facility, it is not possible to store additional effective two-body terms that could arise from $\overline{M1}_{\text{hf}}$ and $\overline{H}_{\text{PT}}$. Since both $M1_{\text{hf}}$ and H_{PT} are one-body operators, fewer two-body terms will arise from $\overline{M1}_{\text{hf}}$ and $\overline{H}_{\text{PT}}$ compared to $\overline{H}_0$. Thus, their effective one-body diagrams are only computed and stored for further use in the above equations, while their effective two-body terms are computed directly. In the last equation, we compute effective one-body terms of $\overline{H}_0 T^{(1,0)} + \overline{M1}_{\text{hf}}$ together, then multiply by $T^{(0,1)}$ to economically compute the $\overline{H}_0 T^{(1,0)} T^{(0,1)}$ and $\overline{M1}_{hf} T^{(0,1)}$ terms. In the RCCSD method approximation, we write

$$T^{(1,0)} = T_1^{(1,0)} + T_2^{(1,0)},$$
$$T^{(0,1)} = T_1^{(0,1)} + T_2^{(0,1)},$$

and

$$T^{(1,1)} = T_1^{(1,1)} + T_2^{(1,1)}. \quad (44)$$

With the knowledge of $T^{(1,0)}$, $T^{(0,1)}$, and $T^{(1,1)}$ amplitudes, we can evaluate the second-order EDM enhancement factors as

$$\frac{d_a^{\text{2nd}}}{\lambda_2} \simeq 2\frac{\langle\Phi_0|e^{T^{(0,0)\dagger}} D e^{T^{(0,0)}} T^{(0,1)}|\Phi_0\rangle}{\langle\Phi_0|e^{T^{(0,0)\dagger}} e^{T^{(0,0)}}|\Phi_0\rangle}$$
$$\simeq 2\langle\Phi_0|\widetilde{D} T^{(0,1)}|\Phi_0\rangle_l, \quad (45)$$

where $\widetilde{D} = e^{T^{(0,0)\dagger}} D e^{T^{(0,0)}}$. As can be seen, the normalization of the wave function has been canceled with the unlinked terms of $\widetilde{D}$ in the above expression, leaving out only the linked terms for the final evaluation. This argument can be followed from the discussions given in Refs. [82,83] and this is further verified using the biorthogonal condition [29,84]. Proceeding in a similar manner, the third-order EDM enhancement factors can be evaluated using the expression

$$\frac{d_a^{\text{3rd}}}{\lambda_1\lambda_2} \simeq 2\langle\Phi_0|\widetilde{D} T^{(1,1)} + T^{(1,0)\dagger}\widetilde{D} T^{(0,1)}|\Phi_0\rangle_l. \quad (46)$$

We adopt an iterative procedure to evaluate the contributions from $\widetilde{D}$ self-consistently. Once $\widetilde{D}$ is computed and stored, each term is reduced to a terminated expression in both Eqs. (45) and (46) in the RCCSD method approximation to obtain the final result.

V. RESULTS AND DISCUSSION

Before presenting the results from various P,T-odd interaction sources to the EDM of ^{129}Xe, it is important to validate the calculations. There are two aspects to be looked into in such intent—completeness of basis functions used in the generation of atomic orbitals and reproducing some known quantities (i.e., comparing between the calculated and experimental results) using the determined wave functions. It is challenging to deal with basis functions in the calculations of atomic properties as it is not possible to obtain a complete set of basis

functions to estimate a property of our interest. In the consideration of finite-size basis functions, they are chosen keeping in view the sensitivity of a given property at the shorter or longer radial distances. The matrix elements of the D operator are more sensitive to the wave functions at the longer distances. However, the P,T-odd interactions of our interest originate from the nucleus. The s and $p_{1/2}$ orbital wave functions having larger overlap with the nucleus are supposed to be predominantly contributing to the matrix elements of H_{PT}.

It may not be necessary to use a sufficient number of orbitals from a higher orbital angular momentum, i.e., $l > 1$. Again, the energy denominators can also play crucial roles in deciding the important contributing high-lying orbitals to the perturbative quantities. Thus, it is expected that contributions from the ns and $np_{1/2}$ orbitals with principal quantum number $n > 20$ to the EDM may not be large. This argument may be valid in the determination of the d_a^{2nd} values, but one has to be careful with such presumption in the evaluation of the d_a^{3rd} contributions. This is because the third-order contributions to the EDM of ^{129}Xe can be enhanced by the $\langle ns|M1_{hf}|ms\rangle$ and $\langle np_{1/2}|M1_{hf}|mp_{1/2}\rangle$ matrix elements with continuum orbitals lying beyond $n, m > 20$ due to the fact that these orbitals have large overlap within the nuclear region, and energy differences between the associated ns and $np_{1/2}$ orbitals do not appear in the denominator of the terms involving the $\langle ns|M1_{hf}|ms\rangle$ and $\langle np_{1/2}|M1_{hf}|mp_{1/2}\rangle$ matrix elements.

It is possible to verify enhancement to the EDM contributions from these high-lying orbitals using the DHF method or using an all-order method such as random phase approximation (RPA), as these methods do not require much computational resources. On the point about determining some quantities and comparing them with their experimental values, it would be desirable to search for properties having similarities with the EDM calculations. However, evaluation of the EDM involves the matrix elements of D, the matrix elements of H_{PT} (via $|\Psi_0^{(0,1)}\rangle$ and $|\Psi_0^{(1,1)}\rangle$), and the excitation energies (appearing in the denominator of the amplitude coefficients of the perturbed wave function). There is no such measurable property of ^{129}Xe known which has a striking similarity with the calculation of its EDM. In the open-shell EDM studies, one evaluates hyperfine-structure constants and electric dipole polarizabilities (α_d) obtained using the calculated wave functions to compare them with their available experimental values for testing the accuracy of the atomic wave functions in the nuclear and asymptotic regions, respectively. Since the ground state of ^{129}Xe does not have hyperfine splitting, we only determine its α_d and compare it with the experimental value [85]. The same has also been done earlier while calculating contributions from the P,T-odd interactions to the atomic EDM of ^{129}Xe [29,82,86,87].

It is well known in the literature that the Gaussian type of orbitals (GTOs) form a good set of basis functions that can describe wave functions near the nuclear region very well [88–90]. We have also used the Fermi nuclear charge distribution [91] to define $\rho_N(r)$ and the nuclear potential. We have used 40 GTOs using an even tempering condition, as described in [92], for each orbital belonging to l values up to 4 (i.e., g symmetry) in the present calculation. There are two reasons for not considering orbitals from the higher momentum values. First, these omitted orbitals do not contribute

TABLE I. Calculated values of α_d (in a.u.), d_a^{Sm} (in $\times 10^{-17} \frac{S}{e\,\mathrm{fm}^3}\,e\,\mathrm{cm}$), d_a^T (in $\times 10^{-20}\langle\sigma\rangle C_T\,e\,\mathrm{cm}$), d_a^{Ps} (in $\times 10^{-23}\langle\sigma\rangle C_P\,e\,\mathrm{cm}$), d_a^B (in $\times 10^{-4}\,e\,\mathrm{cm}$), d_a^e (in $\times 10^{-4}\,e\,\mathrm{cm}$), and d_a^{Sc} [in $\times 10^{-23}(C_S/A)\,e\,\mathrm{cm}$] from our DHF, RPA, and RCCSD methods. Results from previous studies are also given, including the measured value of α_d [85]. We have used nuclear magnetic moment $\mu = -0.777976\mu_N$ and nuclear spin $I = 1/2$ in the estimation of the hyperfine-induced contributions.

Quantity	This work				Others
	DHF	RPA	RCCSD	Final	
α_d	26.866	26.975	27.515	27.55(30)	
					27.782(50) [82]
					27.51 [29]
					25.58 [86]
d_a^{Sm}	0.289	0.378	0.345	0.337(10)	0.38 [87]
					0.337(4) [82]
					0.32 [29]
d_a^T	0.447	0.564	0.522	0.510(10)	0.41 [26]
					0.519 [27]
					0.501(2) [82]
					0.49 [29]
					0.507(48) [86]
					0.57 [87]
d_a^{Ps}	1.287	1.631	1.504	1.442(25)	1.6 [87]
d_a^B	0.669	0.795	0.745	0.716(15)	1.0 [87]
					0.869 [27]
d_a^e	10.171	12.075	11.205	10.75(25)	−8.0 [26]
					−9.361[a] [27]
d_a^{Sc}	3.545	4.439	4.032	3.91(10)	0.71(18) [86]

[a]Unit is changed from the original reported value using $\mu = -0.77686\mu_N$ quoted in Ref. [27].

up to the desired precision to the EDM of ^{129}Xe. Second, evaluation of d_a^{3rd} demands the inclusion of higher s and p continuum orbitals to obtain a reliable result for the EDM. So inclusion of higher angular momentum orbitals to account for electron correlation effects in the RCCSD method would be a challenge with the available computational facilities; especially the orbitals with $l > 4$, which are not significantly contributing to the matrix elements of H_{PT}. We also demonstrate in this work a set of basis functions that would be sufficient to provide accurate value of α_d, but not sufficient enough to correctly estimate the d_a^{3rd} contributions. In view of the aforementioned discussions, it would be necessary to investigate the convergence of the d_a^{3rd} contributions to the EDM by considering as many ns and $np_{1/2}$ orbitals as possible in the calculations.

In Table I, we summarize the calculated α_d, d_a^{2nd}, and d_a^{3rd} values of ^{129}Xe from the DHF, RPA, and RCCSD methods. The reason for giving results from RPA is that the previous calculations were mostly reported results using this approach. Again, differences between the DHF and RPA results will indicate the roles of core-polarization contributions, while differences between the RPA and RCCSD results would exhibit the roles of non-core-polarization contributions in the determination of the investigated quantities. It can be seen from the table that differences between the DHF, RPA, and RCCSD values are not so significant though non-negligible

in all the evaluated properties. It means that the correlation effects in this atom are not very strong. It can also be noticed that the α_d value increases from the DHF method to RPA, then from RPA to the RCCSD method. However, the d_a^{2nd} values show different trends—these values increase from the DHF method to RPA, then they decrease slightly in the RCCSD method. Since the RCCSD method implicitly contains all the RPA effects [82], it implies that the non-RPA effects arising through the RCCSD method behave differently in the determination of α_d and d_a^{2nd}.

The d_a^{3rd} values also show similar trends, i.e., first they increase from the DHF method to RPA, then decrease slightly in the RCCSD method. However, the correlation effects are relatively smaller in magnitude for the d_a^{3rd} values compared to the d_a^{2nd} values. Therefore, it is very important that the DHF values for d_a^{3rd} are reliably determined in order to estimate their final values more accurately using the RCCSD method. We also give our final values along with their possible uncertainties from the neglected contributions. The final results are estimated by including contributions from the Breit and lower-order QED interactions to the RCCSD values, which are then compared with the previous calculations reported in Refs. [26,27,29,82,86,87]. Uncertainties in all the quantities are estimated by analyzing the variation in the results due to use of the finite-size basis functions, approximations in the many-body methods, nuclear model parameters, and QED model potential. These sources of errors contribute with a different amount in each calculated quantity.

The calculated α_d values from the same methods, which are employed to obtain the EDM results, are also compared with the experimental result [85] in Table I. It shows that our calculated value α_d agrees well with the experimental result. They also match with our previous calculations [29,82], where smaller-size basis functions were used and contributions from the Breit and QED effects were neglected. However, our α_d value differs substantially from the value reported in Ref. [86] using the configuration interaction (CI) method. In fact, the CI value is found to be smaller than our DHF and RPA results. From the comparison of the EDM results, we find our RPA values for d_a^{Sm}, d_a^T, and d_a^{Ps} match with the RPA values listed in Ref. [87]. However, we find our RPA value for d_a^B differs from Ref. [87], while it is almost in agreement with the RPA value given in Ref. [27]. A careful analysis of this result suggests that the calculation of d_a^B is very sensitive to the choices of root-mean-square radius R and radial integral limits in the evaluation of the single matrix elements of h_k^B, as explicitly demonstrated later. Our RCCSD values for all of these quantities agree with the RCCSD results and calculations using the normal relativistic coupled-cluster theory reported in Refs. [29,82].

After discussing the second-order perturbative properties, we now move on to discuss the d_a^e and d_a^{Sc} values. Unlike the properties discussed earlier, we find that our third-order properties differ significantly from the previously reported values. The reported d_a^e value in Ref. [27] was performed at the RPA level, while it was obtained analytically in Ref. [26]. The d_a^{Sc} value of Ref. [86] was estimated using the CI method. In the case of d_a^e, we observe a sign difference between our result and that reported in Refs. [27,86]. On the other hand, the signs of our calculated d_a^{Sc} value agree with the result of

Ref. [86]. Since there is an analytical relationship between the S-Ps and electron EDM P,T-odd interaction Hamiltonians, the signs of both contributions are anticipated to be the same. From this analysis, we assume that the sign of our estimated value for d_a^e is right.

Now looking into large differences in the magnitudes for these d_a^{3rd} contributions, we find that they are due to the different basis functions used in the calculations. This can also be corroborated from the fact that the correlation effects arising through the RCCSD method to the d_a^{3rd} contributions are not as large, and thus the main differences in the results come from the DHF values. The magnitudes of the d_a^e value among various calculations almost agree, but there is an order of magnitude difference for d_a^{Sc}. The authors have analyzed the roles of the basis functions in the determination of α_d, d_a^T, and d_a^{Sc} in Ref. [86]. They have noticed large fluctuations in the results, and their final α_d value (i.e., 25.58 a.u.) differs significantly from the experiment. Also, they have made a small virtual cutoff to manage the calculations with the limited computational resources as the CI method can demand for huge RAM in the computers for direct diagonalization with a bigger size configuration space. We demonstrate below, using both the DHF and RPA methods, how such cutoff for the virtual orbitals does not significantly affect the determination of the d_a^{2nd} values, but they are very sensitive to the evaluation of the d_a^{3rd} values.

We present the DHF values for α_d, d_a^{2nd}, and d_a^{3rd} of ^{129}Xe in Table II from a different set of single-particle orbitals. Since the s, $p_{1/2}$, and $p_{3/2}$ orbitals are the dominantly contributing orbitals, we consider these orbitals first and gradually include orbitals with higher orbital angular momentum values, until the g symmetries, to show their roles in the determination of the above quantities. At this stage, it is important to note that some of the orbitals from the higher angular momentum may not contribute through the DHF method, but they can contribute via the electron correlation effects to the above quantities. Thus, if the correlation effects are significant in the determination of the investigated properties only, then one needs to worry about the contributions from the higher angular momentum (belonging to $l > 4$) orbitals to the calculations. Anyway, later we shall present a variation of correlation effects through the RPA method considering a few typical sets of orbitals to show how inclusion of orbitals from the higher angular momentum can affect the results.

In Table II, we start presenting results considering $20s$, $20p_{1/2}$, and $20p_{3/2}$ orbitals (set I). This is a reasonable size basis function when only the s and p orbitals make dominant contributions to a property. The results reported from this set of basis functions are already close to the DHF values for all the d_a^{2nd} values, whereas there is a large difference seen for the α_d value from the final value of the DHF method quoted in Table II. We also see quite significant differences for the d_a^{3rd} values at the DHF method compared to what are listed in Table II. This shows that contributions from the other orbitals are also substantial to the evaluation of the α_d and d_a^{3rd} values, but their contributions are small for d_a^{2nd}. To learn how the high-lying ns and np continuum orbitals, or orbitals with the higher orbital angular momentum, can affect the results, we consider two more sets of basis functions in the next step by including $35s$ and $35p$ orbitals (set II), then increase them up

TABLE II. Convergence of the DHF values for the estimated α_d and EDM enhancement factors from various P,T-odd interactions in ^{129}Xe with different sizes of basis functions, which are identified as set number (Set no.).

Set no.	Basis size	α_d (a.u.)	$d_a^{Sm} \times 10^{-17}$ $[S/(e\,\text{fm}^3)\,e\,\text{cm}]$	$d_a^T \times 10^{-20}$ $(\langle\sigma\rangle C_T\,e\,\text{cm})$	$d_a^{Ps} \times 10^{-23}$ $(\langle\sigma\rangle C_P\,e\,\text{cm})$	$d_a^B \times 10^{-4}$ $e\,\text{cm}$	$d_a^e \times 10^{-4}$ $e\,\text{cm}$	$d_a^{Sc} \times 10^{-23}$ $[(C_S/A)\,e\,\text{cm}]$
I	$20s, 20p$	4.282	0.289	0.446	1.286	0.676	0.640	0.051
II	$30s, 30p$	4.282	0.290	0.447	1.287	0.675	8.718	2.017
III	$35s, 35p$	4.282	0.290	0.447	1.287	0.675	9.917	3.542
IV	$40s, 40p$	4.282	0.290	0.447	1.287	0.675	9.918	3.547
V	$35s, 35p, 35d$	25.978	0.289	0.447	1.287	0.669	10.171	3.545
VI	$40s, 40p, 40d$	25.978	0.289	0.447	1.287	0.669	10.172	3.550
VII	$40s, 40p, 40d, 40f, 40g$	26.868	0.289	0.447	1.287	0.669	10.172	3.550
VIII	*$35s, 35p, 35d, 15f, 15g$*	*26.866*	*0.289*	*0.447*	*1.287*	*0.669*	*10.171*	*3.545*
IX	$20s, 20p, 20d, 15f, 15g$	26.866	0.289	0.447	1.287	0.670	0.651	0.051

to $40s$ and $40p$ orbitals (set III). It shows that none of the $d_a^{2\text{nd}}$ values as well as α_d make much change with the inclusion of more ns and np orbitals, but the $d_a^{3\text{rd}}$ values change by one order with the inclusion of $35s$ and $35p$ orbitals and get saturated after that. This strongly advocates for the fact that the roles of the continuum orbitals beyond $n > 20$ are very crucial for an accurate estimation of the $d_a^{3\text{rd}}$ values. We proceed further by adding orbitals from the higher angular momentum. We consider $35d$ orbitals first, along with $35s$ and $35p$ orbitals (set IV), then $40d$ orbitals, along with $40s$ and $40p$ orbitals (set V). The DHF values in both cases seem to be almost the same for all of these quantities. Compared with the previous set of orbitals, we find that none of the $d_a^{2\text{nd}}$ and $d_a^{3\text{rd}}$ values change, except the α_d value. This asserts our earlier statement about how the EDM results are sensitive to only the higher ns and np orbitals, but contributions from the other orbitals to the EDM are negligibly small. Nonetheless, orbitals from the g symmetry do not contribute for the DHF method, as there are no occupied orbitals present in the f shell of ^{129}Xe, while virtual f orbitals contribute due to the presence of the occupied d orbitals. Their contributions to the EDM are negligible, while a small contribution from these orbitals is noticed in the determination of α_d.

In the present work, we have used the Fermi-type nuclear charge distribution, given by

$$\rho(r) = \frac{\rho_0}{1 + e^{(r-b)/a}}, \quad (47)$$

where ρ_0 is a normalization constant, b is the half-charge radius, and $a = 2.3/4\ln(3)$ is related to the skin thickness. The relation between R, b, and a is given by

$$R = \sqrt{\frac{3}{5}b^2 + \frac{7}{5}a^2\pi^2}. \quad (48)$$

In Table III, we show how the DHF value for d_a^B changes with R (by varying the b value) and cutoff in the radial integration of the wave functions with the basis set VIII. As can be seen from the table, for a small radial integral cutoff, the results show opposite signs than with the larger cutoffs. The value increases until 200 a.u., then slightly decreases at the very large cutoff values. Beyond 500 a.u., we do not see any further changes in the results. Again, we see significant variation in the results with b values. In our calculation, we use $b = 5.655$

fm, at which it satisfies the empirical relation

$$R = 0.836A^{1/3} + 0.570 \text{ fm}, \quad (49)$$

where A is the atomic mass of ^{129}Xe. Thus, one of the reasons for the difference in the d_a^B value between the present work and that reported in [26,27] could be due to the choices of different nuclear charge radii and cutoff in the radial integration of the matrix elements.

We also verify how the hyperfine-induced results differ without and with considering the magnetization distribution [$\mathcal{M}(r)$] within the nucleus. In this case too, we use the Fermi-type distribution as

$$\mathcal{M}(r) = \frac{1}{1 + e^{(r-b)/a}}. \quad (50)$$

The DHF values for d_a^e and d_a^{Sc} without and after multiplying the above factor with the $M1_{\text{hf}}$ operator are given in Table IV. As can be seen from the table, there is a significant reduction in the magnitudes of the above quantities when the magnetization distribution is taken into account within the nucleus. Our final results, reported in Table I, include these effects.

In order to analyze how the high-lying orbitals enhance the $d_a^{3\text{rd}}$ contributions in the DHF method, we take the help of Goldstone diagrams as have been described in Ref. [27]. In Fig. 1, we show these Goldstone diagrams representing six terms of the DHF method that contribute to $d_a^{3\text{rd}}$. We present contributions from these diagrams in Table V using four representative sets of basis functions that are denoted as sets I, II, III, V, and VIII in Table II. We have also compared our results diagramwise from the bigger basis (set VIII) with the results from Ref. [27]. As can be seen from the table, the result

TABLE III. Change in the DHF value for d_a^B (in $\times 10^{-4}$) for different values of b. We have used the basis set VIII and fixed a as 0.523 387 555 fm to carry out the analysis.

R value	b value (fm)			
(a.u.)	5.605	5.625	5.655	5.695
30	-2.241	-2.188	-2.108	-2.001
100	0.581	1.429	1.365	1.281
200	1.044	1.006	0.949	0.874
500	0.927	0.721	0.669	0.600

TABLE IV. The DHF values for d_a^e and d_a^{Sc} from the basis set VIII without and after considering the nuclear magnetization distribution.

Condition	$d_a^e \times 10^{-4}$ e cm	$d_a^{Sc} \times 10^{-23}$ $[(C_S/A)\,e\,\text{cm}]$
Without	11.007	4.624
With	10.171	3.545

from set I that gives very small DHF values to d_a^{3rd} produces reasonable contributions via Figs. 1(i), 1(iv), 1(v), and 1(vi). In all of these cases, the matrix elements of H_{PT} and $M1_{hf}$ are involved with at least one core orbital. The remaining two diagrams involve the matrix elements of H_{PT} and $M1_{hf}$ between the virtual orbitals whose energy denominators do not appear in the evaluation of the DHF value. This ascertains our initial discussion about why the high-lying virtual orbitals enhance the d_a^{3rd} contributions. Compared to the results from Ref. [27], we find that our results from Figs. 1(i), 1(v), and 1(vi) match quite well (only the magnitude, but sign differs as was mentioned earlier), while they differ for the other diagrams. We also find that the result trends from different DHF diagrams are different for d_a^e and d_a^{Sc}. This is clearly evident from the contributions of Figs. 1(ii) and 1(iii), where basis sets I and II give small values for both quantities. With the basis set VIII, the contribution to the d_a^e value becomes almost three times as large, while it only increases marginally for d_a^{Sc}. Thus, we infer from these discussions that a consideration of a very large set of basis functions in the estimations of the hyperfine-induced contributions to the atomic EDM is crucial.

As stated earlier, the correlation effects between the d, f, and g orbitals through the DHF potential are absent for the calculations of the above quantities. However, their correlation effects through the residual Coulomb interaction may affect the results through the RPA and RCCSD methods. To verify this fact, we make a similar analysis in the trends of the results from different interactions by performing RPA calculations with the previously used basis sets. These results are listed in Table VI, from which it can be seen that the all-order method
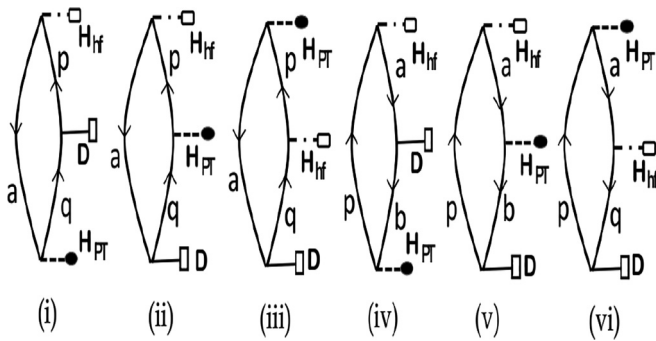
TABLE V. Contributions from different DHF diagrams to the d_a^{3rd} values using four representative basis functions. Values from d_a^e and d_a^{Sc} are given in $\times 10^{-4}\,e$ cm and $\times 10^{-23}(C_S/A)\,e$ cm, respectively.

Fig. no.	Basis set	d_a^e value This work	d_a^e value Ref. [27]	d_a^{Sc} value
Fig. 1(i)	I	−0.878		−0.054
	II	−0.874		−0.054
	III	−0.874		−0.054
	V	−0.872		−0.054
	VIII	*−0.872*	0.870	−0.054
Fig. 1(ii)	I	1.664		1.021
	II	5.675		1.061
	III	6.288		1.832
	V	6.338		1.833
	VIII	*6.338*	−4.887	1.833
Fig. 1(iii)	I	3.109		0.200
	II	7.170		1.203
	III	7.757		1.957
	V	7.948		1.959
	VIII	*7.948*	−6.697	1.959
Fig. 1(iv)	I	0.890		0.055
	II	0.892		0.055
	III	0.892		0.055
	V	0.893		0.055
	VIII	*0.893*	−0.963	0.055
Fig. 1(v)	I	−2.870		−0.172
	II	−2.870		−0.172
	III	−2.870		−0.172
	V	−2.861		−0.171
	VIII	*−2.861*	2.859	−0.171
Fig. 1(vi)	I	−1.275		−0.077
	II	−1.275		−0.077
	III	−1.275		−0.077
	V	−1.274		−0.077
	VIII	*−1.274*	1.274	−0.077

FIG. 1. Diagrammatic representation of different DHF contributions to the d_a^{3rd} values. Lines with upward arrows denote virtual orbitals and lines with downward arrows denote occupied orbitals. Operators H_{hf}, H_{PT}, and D are shown by a singled dotted line with a rectangular box, a dotted line with a black circle, and a line with a square, respectively.

also shows similar trends in the results as in the DHF method. From this exercise, it follows that orbitals with higher angular momentum do not significantly contribute to the d_a^{2nd} and d_a^{3rd} contributions and consideration of the high-lying ns and np orbitals with $n > 20$ are essential for an accurate estimate of the d_a^{3rd} contributions.

In Table VII, we present contributions from the individual terms of the RCCSD method to the estimations of α_d and the d_a^{2nd} values from different H_{PT}. We find that $DT_1^{(0,1)}$ and its Hermitian conjugate (H.c.) give almost all the contributions to the above quantities. The next dominant contributions arise through $T_2^{(0,0)\dagger}DT_1^{(0,1)}$ and its H.c. Contributions from the higher-order nonlinear terms ("Others") are non-negligible. At the end of the table, we have also listed contributions arising through the Breit and lower-order QED interactions. They show that the Breit interaction contributes more to α_d than the QED effects, while it is the reverse for d_a^{2nd}.

We also present contributions from the individual terms of the RCCSD method to the estimations of the d_a^{3rd}

TABLE VI. Convergence of the RPA values of the estimated α_d and EDM enhancement factors from various P,T-odd interactions in ^{129}Xe with different size of basis functions.

Set no.	Basis size	α_d (a.u.)	$d_a^{Sm} \times 10^{-17}$ $[S/(e\,\text{fm}^3)\,e\,\text{cm}]$	$d_a^T \times 10^{-20}$ $(\langle\sigma\rangle C_T\,e\,\text{cm})$	$d_a^{Ps} \times 10^{-23}$ $(\langle\sigma\rangle C_P\,e\,\text{cm})$	$d_a^B \times 10^{-4}$ $e\,\text{cm}$	$d_a^e \times 10^{-4}$ $e\,\text{cm}$	$d_a^{Sc} \times 10^{-23}$ $[(C_S/A)\,e\,\text{cm}]$
I	$20s, 20p$	6.753	0.481	0.723	2.088	1.036	0.541	0.052
II	$30s, 30p$	6.753	0.482	0.723	2.088	1.031	13.582	3.234
III	$35s, 35p$	6.753	0.482	0.723	2.088	1.031	15.518	5.504
IV	$40s, 40p$	6.753	0.482	0.723	2.088	1.031	15.519	5.509
V	$35s, 35p, 35d$	26.923	0.379	0.565	1.634	0.794	12.168	4.463
VI	$40s, 40p, 40d$	26.923	0.379	0.565	1.634	0.794	12.172	4.466
VII	$40s, 40p, 40d, 40f, 40g$	26.975	0.379	0.565	1.634	0.794	12.172	4.466
VIII	*$35s, 35p, 15d, 15f, 15g$*	*26.975*	*0.378*	*0.564*	*1.631*	*0.795*	*12.168*	*4.463*
IX	$20s, 20p, 20d, 15f, 15g$	26.975	0.378	0.564	1.631	0.795	0.441	0.051

values in Table VIII. In this case, the $DT_1^{(1,1)}$ + H.c. terms contribute mostly to both d_a^e and d_a^{Sc}, and the next leading-order contributions arise from $T_1^{(0,1)\dagger}DT_1^{(1,0)}$ + H.c. There are non-negligible contributions from $T_2^{(0,1)\dagger}DT_1^{(1,0)}$ + H.c., $T_2^{(0,0)\dagger}DT_2^{(1,1)}$ + H.c., and $T_2^{(0,1)\dagger}DT_2^{(1,0)}$ + H.c. The rest of the contributions ("Others") are also quite significant. At the bottom of the table, we quote contributions from both the Breit and QED interactions. In this case, contributions arising through the QED interactions seem to be relatively large.

The latest reported experimental result for the EDM of ^{129}Xe is [93,94]

$$|d_{\text{Xe}}| < 1.4 \times 10^{-27}\,e\,\text{cm}, \tag{51}$$

where $e = |e|$ is the electric charge. Now, considering our recommended values as

$$d_a = 0.510(10) \times 10^{-20}\langle\sigma\rangle C_T\,e\,\text{cm}$$

and

$$d_a = 0.337(10) \times 10^{-17}\,S/(e\,\text{fm}^3)\,e\,\text{cm}, \tag{52}$$

and combining them with the experimental result for EDM, we obtain limits as

$$|C_T| < 5.9 \times 10^{-7}$$

and

$$|S| < 4.2 \times 10^{-10}\,e\,\text{fm}^3. \tag{53}$$

In deriving the upper limit of $|C_T|$, we took into account the 30% uncertainty of the spin matrix element $\langle\sigma\rangle \approx \langle\sigma_n\rangle \approx 0.66$.

Similarly, considering

$$d_a = 1.442(25) \times 10^{-23}\langle\sigma\rangle C_P\,e\,\text{cm}, \tag{54}$$

we deduce the limit as

$$|C_P| < 2.1 \times 10^{-4}. \tag{55}$$

This follows the ratio of the C_P and C_T values as 0.3559×10^3 that agrees well with the value 0.3556×10^3 estimated using the empirical relation given by Eq. (32).

Now, we can express the above parameters at the hadron level as

$$\left|\bar{g}_{\pi NN}^{(0)}\right| < 1.2 \times 10^{-9},$$
$$\left|\bar{g}_{\pi NN}^{(1)}\right| < 1.1 \times 10^{-9},$$
$$\left|\bar{g}_{\pi NN}^{(2)}\right| < 5.4 \times 10^{-10},$$

and

$$|d_n| < 1.3 \times 10^{-22}\,e\,\text{cm}, \tag{56}$$

where we assumed 30% of nuclear level uncertainty. We do not set a limit for the proton EDM which is affected by large error. When the sensitivity of the ^{129}Xe EDM experiment improves by about three orders of magnitude as expected [95], the resulting NSM limit together with nuclear structure

TABLE VII. Contributions to α_d and d_a^{2nd} enhancement factors from various P,T-odd interactions in ^{129}Xe through individual terms of the RCCSD method. For the terms that are not explicitly shown, their contributions are given together under "Others." Estimated contributions from the Breit and QED interactions are given at the bottom of the table.

RCC terms	α_d (a.u.)	$d_a^{Sm} \times 10^{-17}$ $[S/(e\,\text{fm}^3)\,e\,\text{cm}]$	$d_a^T \times 10^{-20}$ $(\langle\sigma\rangle C_T\,e\,\text{cm})$	$d_a^{Ps} \times 10^{-23}$ $(\langle\sigma\rangle C_P\,e\,\text{cm})$	$d_a^B \times 10^{-4}$ $e\,\text{cm}$
$DT_1^{(0,1)}$ + H.c.	29.980	0.318	0.510	1.471	0.722
$T_1^{(0,0)\dagger}DT_1^{(0,1)}$ + H.c.	−0.345	0.003	0.004	0.017	0.007
$T_2^{(0,0)\dagger}DT_1^{(0,1)}$ + H.c.	−3.308	0.011	0.017	0.049	0.034
$T_1^{(0,0)\dagger}DT_2^{(0,1)}$ + H.c.	0.074	∼0.0	∼0.0	−0.001	−0.001
$T_2^{(0,0)\dagger}DT_2^{(0,1)}$ + H.c.	1.072	∼0.0	∼0.0	−0.001	−0.003
Others	0.042	0.013	−0.009	−0.031	−0.014
Breit	0.051	−0.002	−0.001	−0.003	0.003
QED	−0.015	−0.006	−0.011	−0.059	−0.032

TABLE VIII. Contributions to the $d_{\mathrm{a}}^{\mathrm{3rd}}$ enhancement factors from the electron EDM and S-Ps interactions in ^{129}Xe through individual terms of the RCCSD method. For the terms that are not explicitly shown, their contributions are given together as "Others." The Breit and QED interaction contributions are given at the end of the table.

RCC terms	$d_{\mathrm{a}}^{e} \times 10^{-4}$ $e\,\mathrm{cm}$	$d_{\mathrm{a}}^{Sc} \times 10^{-23}$ $[(C_{\mathrm{S}}/A)\,e\,\mathrm{cm}]$
$DT_1^{(1,1)} + $ H.c.	10.922	3.953
$T_1^{(0,1)\dagger} DT_1^{(1,0)} + $ H.c.	−0.076	−0.004
$T_2^{(0,1)\dagger} DT_1^{(1,0)} + $ H.c.	−0.045	−0.003
$T_1^{(0,1)\dagger} DT_2^{(1,0)} + $ H.c.	0.0	0.0
$T_2^{(0,0)\dagger} DT_2^{(1,1)} + $ H.c.	−0.018	−0.002
$T_2^{(0,1)\dagger} DT_2^{(1,0)} + $ H.c.	−0.020	−0.001
Others	0.428	0.088
Breit	−0.037	−0.008
QED	−0.417	−0.118

calculations will give the improved limits at the quark-gluon level CP violation.

Using the results from the present study, the final expression in terms of all possible contributions can be given for $\mu = 1$ TeV as

$$
\begin{aligned}
d_{\mathrm{Xe}} = {}& 1.15 \times 10^{-3} d_e - 2.6 \times 10^{-6} d_u + 1.0 \times 10^{-5} d_d \\
& + (-2 \times 10^{-20} \bar{\theta} e\,\mathrm{cm}) + 2.4 \times 10^{-3} e(\tilde{d}_d - \tilde{d}_u) \\
& + \big(0.040 C_S^{eu} + 0.041 C_S^{ed} - 0.29 C_P^{eu} + 0.30 C_P^{ed} \\
& - 0.055 C_T^{eu} + 0.22 C_T^{ed}\big) \times 10^{-20} e\,\mathrm{cm},
\end{aligned} \tag{57}
$$

and for $\mu = 1$ GeV as

$$
\begin{aligned}
d_{\mathrm{Xe}} = {}& 1.15 \times 10^{-3} d_e - 3.3 \times 10^{-6} d_u + 1.3 \times 10^{-5} d_d \\
& + (-2 \times 10^{-20} \bar{\theta} e\,\mathrm{cm}) + 2.6 \times 10^{-3} e(\tilde{d}_d - \tilde{d}_u) \\
& + \big(0.020 C_S^{eu} + 0.020 C_S^{ed} - 0.14 C_P^{eu} + 0.15 C_P^{ed} \\
& - 0.070 C_T^{eu} + 0.28 C_T^{ed}\big) \times 10^{-20} e\,\mathrm{cm},
\end{aligned} \tag{58}
$$

where we displayed the cases for two renormalization scales $\mu = 1$ TeV and $\mu = 1$ GeV. The experimental upper limit, given by Eq. (51), is then converted to

$$
\begin{aligned}
|d_e| &< 1.2 \times 10^{-24}\ e\,\mathrm{cm}, \\
|d_u| &< 9.0 \times 10^{-22}\ e\,\mathrm{cm}, \\
|d_d| &< 2.2 \times 10^{-22}\ e\,\mathrm{cm}, \\
|\tilde{d}_u|, |\tilde{d}_d| &< 1.5 \times 10^{-24}\ e\,\mathrm{cm}, \\
\big|C_S^{eu}\big| &< 5.9 \times 10^{-6}, \\
\big|C_S^{ed}\big| &< 5.7 \times 10^{-6}, \\
\big|C_P^{eu}\big| &< 8.2 \times 10^{-7}, \\
\big|C_P^{ed}\big| &< 7.7 \times 10^{-7}, \\
\big|C_T^{eu}\big| &< 4.2 \times 10^{-6},
\end{aligned}
$$

and

$$
\big|C_T^{ed}\big| < 1.0 \times 10^{-6}. \tag{59}
$$

where all elementary level couplings are renormalized at the scale $\mu = 1$ TeV. This is under the assumption of the dominance of only one P,T-odd interaction. We also assumed that the quark EDMs, C_S^{eq}, C_P^{eq}, and C_T^{eq}, are affected by 40% of uncertainty, while the chromo-EDMs by 60%. The above upper limits are looser than those given by other experiments that are given as [96,97]

$$
\begin{aligned}
|d_e| &< 4.1 \times 10^{-30}\ e\,\mathrm{cm}, \\
|d_u| &< 1.2 \times 10^{-25}\ e\,\mathrm{cm}, \\
|d_d| &< 2.9 \times 10^{-26}\ e\,\mathrm{cm}, \\
|\tilde{d}_u|, |\tilde{d}_d| &< 6.4 \times 10^{-28}\ e\,\mathrm{cm}, \\
\big|C_S^{eu}\big| &< 1.9 \times 10^{-11}, \\
\big|C_S^{ed}\big| &< 1.8 \times 10^{-11}, \\
\big|C_P^{eu}\big| &< 6.1 \times 10^{-10}, \\
\big|C_P^{ed}\big| &< 5.7 \times 10^{-10}, \\
\big|C_T^{eu}\big| &< 4.3 \times 10^{-9},
\end{aligned}
$$

and

$$
\big|C_T^{ed}\big| < 9.7 \times 10^{-10}. \tag{60}
$$

VI. CONCLUSION

We have employed the relativistic coupled-cluster theory in the linear response approach to estimate the second- and third-order perturbative contributions due to the parity and time-reversal symmetry violating interactions to the electric dipole moment of ^{129}Xe. We have also compared our results with the previously reported values at the random phase approximation, and performed a calculation of the electric dipole polarizability to verify the reliability of our calculations. We observed contrasting trends of the correlation contributions in the determination of all these quantities. In particular, determination of the third-order perturbative contributions are found to be very sensitive to the contributions from the very high-lying s and $p_{1/2}$ orbitals. In addition, we have also performed nuclear calculations using the shell model. Combining atomic results with the latest experimental value of the electric dipole moment of ^{129}Xe, we inferred the revised limits of the nuclear Schiff moment and the tensor-pseudotensor electron-nucleus coupling coefficient. Using the extracted nuclear Schiff moment with our nuclear calculations, we obtained limits on the pion-nucleon coupling coefficients, and the electric dipole moments of a proton and a neutron. Further, we used all possible second- and third-order perturbative contributions to express the electric dipole moment of ^{129}Xe in terms of the electric dipole moments of electrons and quarks, and the parity and time-reversal violating electron-quark tensor-pseudotensor, pseudoscalar-scalar, and scalar-pseudoscalar coupling coefficients.

APPENDIX: MATRIX

In the Dirac theory, the orbital wave function of an electron, $|\phi_a(r)\rangle$, is given by

$$|\phi_a(r)\rangle = \frac{1}{r}\begin{pmatrix} P_a(r)\chi_{\kappa_a,m_{j_a}}(\theta,\varphi) \\ iQ_a(r)\chi_{-\kappa_a,m_{j_a}}(\theta,\varphi) \end{pmatrix}, \quad \text{(A1)}$$

where $P_a(r)$ and $Q_a(r)$ denote the large and small components of the radial part, and the χ's denote the spin angular parts of each component with relativistic quantum number κ_a, total angular momentum j_a, and its component m_{j_a}.

In terms of these wave functions, the single-particle matrix element of the dipole operator D is given by

$$\langle\kappa_a||d||\kappa_b\rangle = \langle\kappa_a||C^{(1)}||\kappa_b\rangle \int_0^\infty dr(P_aP_b + Q_aQ_b)r, \quad \text{(A2)}$$

where C^1 is the Racah operator of rank 1.

The single-particle matrix element of the electron EDM interaction Hamiltonian is given by

$$\langle j_a||h_k^{d_e}||j_b\rangle = 2c\sqrt{2j_a+1}\,\delta_{\kappa_a,-\kappa_b}\left\{\tilde{l}_a(\tilde{l}_a+1)\int_0^\infty dr\frac{P_a(r)Q_b(r)}{r^2} + l_a(l_a+1)\int_0^\infty dr\frac{Q_a(r)P_b(r)}{r^2}\right.$$
$$\left. + \frac{dP_a(r)}{dr}\frac{dQ_b(r)}{dr} + \frac{dQ_a(r)}{dr}\frac{dP_b(r)}{dr}\right\}, \quad \text{(A3)}$$

where l and $\tilde{l}$ are the orbital quantum number of the large and small component of the Dirac wave function, respectively.

The single-particle matrix elements of the $M1_{\text{hf}}$ operator are given by

$$\langle\kappa_a||t_{hf}^1||\kappa_b\rangle = -(\kappa_a+\kappa_b)\langle-\kappa_a||C^{(1)}||\kappa_b\rangle \int_0^\infty dr\frac{(P_aQ_b+Q_aP_b)}{r^2}, \quad \text{(A4)}$$

where μ_N is the nuclear magneton and g_I is the ratio of nuclear magnetic dipole moment μ_I and I.

The single-particle reduced matrix element of $h^B(r)$ is given by

$$\langle j_a||h_k^B||j_b\rangle = \frac{d_e\mu}{2m_pc}\left\{-3\langle-\kappa_a||C^1||-\kappa_b\rangle\int_R^\infty dr\frac{Q_a(r)P_b(r)}{r^3} - 3\langle\kappa_a||C^1||\kappa_b\rangle\int_R^\infty dr\frac{P_a(r)Q_b(r)}{r^3}\right.$$
$$- \langle-\kappa_a||\sigma_k||\kappa_b\rangle\int_R^\infty dr\frac{Q_a(r)P_b(r)}{r^3} - \langle\kappa_a||\sigma_k||-\kappa_b\rangle\int_R^\infty dr\frac{P_a(r)Q_b(r)}{r^3}$$
$$\left. + 2\langle-\kappa_a||\sigma_k||\kappa_b\rangle\int_0^R dr\frac{Q_a(r)P_b(r)}{r^3} + 2\langle\kappa_a||\sigma_k||-\kappa_b\rangle\int_0^R dr\frac{P_a(r)Q_b(r)}{r^3}\right\}, \quad \text{(A5)}$$

where R is the radius of the nucleus.

The single-particle matrix element for the NSM operator is given by

$$\langle j_a||h_k^{\text{NSM}}||j_b\rangle = \frac{3S}{B}\langle\kappa_a||C_k^{(1)}||\kappa_b\rangle\int_0^\infty dr\rho_{\text{N}}(r)[P_a(r)P_b(r) + Q_a(r)Q_b(r)]. \quad \text{(A6)}$$

The single-particle matrix element of the S-Ps interaction is given by

$$\langle j_a||h_k^{SPs}||j_b\rangle = -\delta_{\kappa_a,-\kappa_b}\frac{G_FC_S}{\sqrt{2}}A\sqrt{2j_a+1}\int_0^\infty dr[P_a(r)Q_b(r) + Q_a(r)P_b(r)]\rho_{\text{N}}(r). \quad \text{(A7)}$$

The single-particle reduced matrix element of the Ps-S operator is given by

$$\langle j_a||h_k^{PsS}||j_b\rangle = -\frac{G_FC_P}{2\sqrt{2}m_pc}\langle\boldsymbol{\sigma}_{\text{N}}\rangle\langle\kappa_a||C^{(1)}||\kappa_b\rangle\int_0^\infty dr[P_a(r)P_b(r) - Q_a(r)Q_b(r)]\frac{d\rho_{\text{N}}(r)}{dr}. \quad \text{(A8)}$$

The single-particle reduced matrix element of the T-Pt operator is given by

$$\langle j_a||h_k^{TPt}||j_b\rangle = -\sqrt{2}G_FC_T\langle\boldsymbol{\sigma}_{\text{N}}\rangle\left[\langle\kappa_a||\sigma_k||-\kappa_b\rangle\int_0^\infty dr\rho_{\text{N}}(r)P_a(r)Q_b(r) + \langle-\kappa_a||\sigma_k||\kappa_b\rangle\int_0^\infty dr\rho_{\text{N}}(r)Q_a(r)P_b(r)\right], \quad \text{(A9)}$$

where σ_k is the Pauli spinor for the electrons.

[1] N. F. Ramsey, Annu. Rev. Nucl. Part. Sci. **32**, 211 (1982).

[2] N. Fortson, P. Sandars, and S. Barr, Phys. Today **56**(6), 33 (2003).

[3] G. R. Farrar and M. E. Shaposhnikov, Phys. Rev. D **50**, 774 (1994).

[4] P. Huet and E. Sather, Phys. Rev. D **51**, 379 (1995).

[5] M. Dine and A. Kusenko, Rev. Mod. Phys. **76**, 1 (2004).

[6] G. Lüders, Ann. Phys. **281**, 1004 (2000).

[7] M. Kobayashi and T. Maskawa, Prog. Theor. Phys. **44**, 1422 (1970).

[8] N. Yamanaka and E. Hiyama, J. High Energy Phys. 02 (2016) 067.

[9] Y. Yamaguchi and N. Yamanaka, Phys. Rev. Lett. **125**, 241802 (2020).

[10] Y. Yamaguchi and N. Yamanaka, Phys. Rev. D **103**, 013001 (2021).

[11] Y. Ema, T. Gao, and M. Pospelov, Phys. Rev. Lett. **129**, 231801 (2022).

[12] S. M. Barr, Int. J. Mod. Phys. A **08**, 209 (1993).

[13] M. Pospelov and A. Ritz, Ann. Phys. **318**, 119 (2005).

[14] M. J. Ramsey-Musolf and S. Su, Phys. Rep. **456**, 1 (2008).

[15] N. Yamanaka, B. K. Sahoo, N. Yoshinaga, T. Sato, K. Asahi, and B. P. Das, Eur. Phys. J. A **53**, 54 (2017).

[16] T. E. Chupp, P. Fierlinger, M. J. Ramsey-Musolf, and J. T. Singh, Rev. Mod. Phys. **91**, 015001 (2019).

[17] S. M. Barr, Phys. Rev. D **45**, 4148 (1992).

[18] X. G. He, B. H. J. McKellar, and S. Pakvasa, Phys. Lett. B **283**, 348 (1992).

[19] U. Mahanta, Phys. Lett. B **337**, 128 (1994).

[20] P. Herczeg, Phys. Rev. D **68**, 116004 (2003); **69**, 039901(E) (2004).

[21] K. Fuyuto, M. Ramsey-Musolf, and T. Shen, Phys. Lett. B **788**, 52 (2019).

[22] W. Dekens, J. de Vries, M. Jung, and K. K. Vos, J. High Energy Phys. 01 (2019) 069.

[23] W. Heil *et al.*, Ann. Phys. **525**, 539 (2013).

[24] F. Kuchler *et al.*, Hyperfine Interact. **237**, 95 (2016).

[25] T. Sato *et al.*, Phys. Lett. A **382**, 588 (2018).

[26] V. V. Flambaum and I. B. Khriplovich, Sov. Phys. JETP **62**, 872 (1985).

[27] A.-M. Mårtensson-Pendrill and P. Öster, Phys. Scr. **36**, 444 (1987).

[28] Y. Singh, B. K. Sahoo, and B. P. Das, Phys. Rev. A **89**, 030502(R) (2014).

[29] A. Sakurai, B. K. Sahoo, K. Asahi, and B. P. Das, Phys. Rev. A **100**, 020502(R) (2019).

[30] J. de Vries, E. Mereghetti, R. G. E. Timmermans, and U. van Kolck, Ann. Phys. **338**, 50 (2013).

[31] J. Bsaisou, U. G. Meißner, A. Nogga, and A. Wirzba, Ann. Phys. **359**, 317 (2015).

[32] Y. H. Song, R. Lazauskas, and V. Gudkov, Phys. Rev. C **87**, 015501 (2013).

[33] N. Yamanaka and E. Hiyama, Phys. Rev. C **91**, 054005 (2015).

[34] P. Froese and P. Navratil, Phys. Rev. C **104**, 025502 (2021).

[35] N. Yamanaka and M. Oka, Phys. Rev. D **106**, 075021 (2022).

[36] N. Yamanaka, S. Hashimoto, T. Kaneko, and H. Ohki, [JLQCD], Phys. Rev. D **98**, 054516 (2018).

[37] R. Gupta, B. Yoon, T. Bhattacharya, V. Cirigliano, Y. C. Jang, and H. W. Lin, Phys. Rev. D **98**, 091501(R) (2018).

[38] C. Alexandrou, S. Bacchio, M. Constantinou, J. Finkenrath, K. Hadjiyiannakou, K. Jansen, G. Koutsou, and A. V. Aviles-Casco, Phys. Rev. D **102**, 054517 (2020).

[39] D. Horkel, Y. Bi, M. Constantinou, T. Draper, J. Liang, K. F. Liu, Z. Liu, and Y. B. Yang (χQCD Collaboration), Phys. Rev. D **101**, 094501 (2020).

[40] R. Tsuji, N. Tsukamoto, Y. Aoki, K. I. Ishikawa, Y. Kuramashi, S. Sasaki, E. Shintani, and T. Yamazaki (PACS Collaboration), Phys. Rev. D **106**, 094505 (2022).

[41] G. S. Bali, S. Collins, S. Heybrock, M. Löffler, R. Rödl, W. Söldner, and S. Weishäupl, Phys. Rev. D **108**, 034512 (2023).

[42] G. Degrassi, E. Franco, S. Marchetti, and L. Silvestrini, J. High Energy Phys. 11 (2005) 044.

[43] C. Cocuzza, A. Metz, D. Pitonyak, A. Prokudin, N. Sato, and R. Seidl, arXiv:2306.12998.

[44] W. C. Haxton and E. M. Henley, Phys. Rev. Lett. **51**, 1937 (1983).

[45] I. S. Towner and A. C. Hayes, Phys. Rev. C **49**, 2391 (1994).

[46] J. de Vries, E. Epelbaum, L. Girlanda, A. Gnech, E. Mereghetti, and M. Viviani, Front. Phys. **8**, 218 (2020).

[47] W. Y. Ai, J. S. Cruz, B. Garbrecht, and C. Tamarit, Phys. Lett. B **822**, 136616 (2021).

[48] Y. Nakamura and G. Schierholz, Nucl. Phys. B **986**, 116063 (2023).

[49] N. Yamanaka, arXiv:2212.10994.

[50] N. Yamanaka, arXiv:2212.11820.

[51] R. J. Crewther, P. Di Vecchia, G. Veneziano, and E. Witten, Phys. Lett. B **88**, 123 (1979).

[52] J. de Vries, E. Mereghetti, and A. Walker-Loud, Phys. Rev. C **92**, 045201 (2015).

[53] N. Yamanaka and E. Hiyama, Phys. Rev. D **103**, 035023 (2021).

[54] N. Osamura, P. Gubler, and N. Yamanaka, J. High Energy Phys. 06 (2022) 072.

[55] M. Abramczyk, S. Aoki, T. Blum, T. Izubuchi, H. Ohki, and S. Syritsyn, Phys. Rev. D **96**, 014501 (2017).

[56] T. Bhattacharya, V. Cirigliano, R. Gupta, E. Mereghetti, J. S. Yoo, and B. Yoon, arXiv:2304.09929.

[57] M. Pospelov, Phys. Lett. B **530**, 123 (2002).

[58] J. Bsaisou, J. de Vries, C. Hanhart, S. Liebig, U. G. Meissner, D. Minossi, A. Nogga, and A. Wirzba, J. High Energy Phys. 03 (2015) 104; Erratum: 05 (2015) 083.

[59] N. Yamanaka, Intl. J. Mod. Phys. E **26**, 1730002 (2017).

[60] J. de Vries, E. Mereghetti, C. Y. Seng, and A. Walker-Loud, Phys. Lett. B **766**, 254 (2017).

[61] V. M. Belyaev and B. L. Ioffe, Sov. Phys. JETP **56**, 493 (1982).

[62] B. L. Ioffe, Prog. Part. Nucl. Phys. **56**, 232 (2006).

[63] P. Gubler and D. Satow, Prog. Part. Nucl. Phys. **106**, 1 (2019).

[64] R. Gupta, S. Park, M. Hoferichter, E. Mereghetti, B. Yoon, and T. Bhattacharya, Phys. Rev. Lett. **127**, 242002 (2021).

[65] A. Agadjanov, D. Djukanovic, G. von Hippel, H. B. Meyer, K. Ottnad, and H. Wittig, arXiv:2303.08741.

[66] B. L. Huang and J. Ou-Yang, Phys. Rev. D **101**, 056021 (2020).

[67] M. Hoferichter, J. R. de Elvira, B. Kubis, and U. G. Meißner, Phys. Rep. **625**, 1 (2016).

[68] K. Yanase, N. Yoshinaga, K. Higashiyama, and N. Yamanaka, Phys. Rev. D **99**, 075021 (2019).

[69] K. Yanase *et al.*, Phys. Lett. B **841**, 137897 (2023).

[70] B. A. Brown, N. J. Stone, J. R. Stone, I. S. Towner, and M. Hjorth-Jensen, Phys. Rev. C **71**, 044317 (2005).

[71] M. S. R. Laskar, S. Saha, R. Palit, S. N. Mishra, N. Shimizu, Y. Utsuno, E. Ideguchi, Z. Naik, F. S. Babra, S. Biswas, S. Kumar, S. K. Mohanta, C. S. Palshetkar, P. Singh, and P. C. Srivastava, Phys. Rev. C **99**, 014308 (2019).

[72] K. Yanase, Phys. Rev. C **103**, 035501 (2021).

[73] K. Yanase and N. Shimizu, Phys. Rev. C **102**, 065502 (2020).

[74] N. Shimizu, T. Mizusaki, Y. Utsuno, and Y. Tsunoda, Comput. Phys. Commun. **244**, 372 (2019).

[75] V. V. Flambaum and J. S. M. Ginges, Phys. Rev. A **65**, 032113 (2002).

[76] E. A. Hinds and P. G. H. Sandars, Phys. Rev. A **21**, 471 (1980).

[77] A.-M. Mårtensson-Pendrill, Phys. Rev. Lett. **54**, 1153 (1985).

[78] J. S. M. Ginges and V. V. Flambaum, Phys. Rep. **397**, 63 (2004).

[79] T. Helgaker, P. Jorgensen, and J. Olsen, *Molecular Electronic Structure Theory* (Wiley, New York, 2000).

[80] T. D. Crawford and H. F. Schaefer III, *An Introduction to Coupled Cluster Theory for Computational Chemists*, Reviews in Quantum Chemistry, edited by K. B. Lipkowitz and D. B. Boyd (Wiley-VCH, New York, 2000), Vol. 14, pp. 33.

[81] I. Shavitt and R. J. Bartlett, *Many-Body Methods in Chemistry And Physics* (Cambridge University Press, Cambridge, 2009).

[82] Y. Singh and B. K. Sahoo, Phys. Rev. A **91**, 030501(R) (2015).

[83] B. K. Sahoo and Y.-M. Yu, Phys. Rev. A **98**, 012513 (2018).

[84] B. K. Sahoo and B. P. Das, Phys. Rev. Lett. **120**, 203001 (2018).

[85] U. Hohm and K. Kerl, Mol. Phys. **69**, 819 (1990).

[86] T. Fleig and M. Jung, Phys. Rev. A **103**, 012807 (2021).

[87] V. A. Dzuba, V. V. Flambaum, and S. G. Porsev, Phys. Rev. A **80**, 032120 (2009).

[88] S. F. Boys, Proc. R. Soc. London A **200**, 542 (1950).

[89] A. K. Mohanty and E. Clementi, Chem. Phys. Lett. **157**, 348 (1989).

[90] K. G. Dyall and K. Fægri, Theoret. Chim. Acta **94**, 39 (1996).

[91] G. Estevez and L. B. Bhuiyan, Am. J. Phys. **53**, 450 (1985).

[92] M. W. Schmidt and K. Ruedenberg, J. Chem. Phys. **71**, 3951 (1979).

[93] F. Allmendinger, I. Engin, W. Heil, S. Karpuk, H. J. Krause, B. Niederländer, A. Offenhäusser, M. Repetto, U. Schmidt, and S. Zimmer, Phys. Rev. A **100**, 022505 (2019).

[94] N. Sachdeva, I. Fan, E. Babcock, M. Burghoff, T. E. Chupp, S. Degenkolb, P. Fierlinger, S. Haude, E. Kraegeloh, W. Kilian and S. Knappe-Grüneberg, F. Kuchler, T. Liu, M. Marino, J. Meinel, K. Rolfs, Z. Salhi, A. Schnabel, J. T. Singh, S. Stuiber, W. A. Terrano, L. Trahms, and J. Voigt, Phys. Rev. Lett. **123**, 143003 (2019).

[95] W. A. Terrano and M. V. Romalis, Quantum Sci. Technol. **7**, 014001 (2022).

[96] T. S. Roussy, L. Caldwell, T. Wright, W. B. Cairncross, Y. Shagam, K. B. Ng, N. Schlossberger, S. Y. Park, A. Wang, J. Ye *et al.*, Science **381**, 46 (2023).

[97] B. Graner, Y. Chen, E. G. Lindahl, and B. R. Heckel, Phys. Rev. Lett. **116**, 161601 (2016); **119**, 119901(E) (2017).